J. Fluid Mech. (1973), *vol.* 60, *part* 1, *pp.* 141–159
Printed in Great Britain

Turbulent convection in a horizontal layer of water

By T. Y. CHU

Western Electric Co. Inc., Engineering Research Center, Princeton, New Jersey

AND R. J. GOLDSTEIN

Department of Mechanical Engineering, University of Minnesota, Minneapolis

(Received 21 July 1972 and in revised form 24 April 1973)

Overall heat transfer and mean temperature distribution measurements have been made of turbulent thermal convection in horizontal water layers heated from below. The Nusselt number is found to be proportional to $Ra^{0.278}$ in the range $2{\cdot}76 \times 10^5 < Ra < 1{\cdot}05 \times 10^8$. Eight discrete heat flux transitions are found in this Rayleigh number range. An interferometric method is used to measure the mean temperature distribution for Rayleigh numbers between $3{\cdot}11 \times 10^5$ and $1{\cdot}86 \times 10^7$. Direct visual and photographic observations of the fluctuating interferogram patterns show that the main heat transfer mechanism is the release of thermals from the boundary layers. For relatively low Rayleigh numbers (up to 5×10^5) many of the thermals reach the opposite surface and coalesce to form large masses of relatively warm fluid near the cold surface and masses of cold fluid near the warm surface, resulting in a temperature-gradient reversal. With increasing Rayleigh numbers, fewer and fewer thermals reach the opposite bounding surface and the thermals show persistent horizontal movements near the bounding surfaces. The central region of the layer becomes an isothermal core. The mean temperature distributions for the high Rayleigh number range are found to follow a Z^{-2} power law over a considerable range, where Z is the distance from the bounding surface. A very limited agreement with the theoretically predicted Z^{-1} power law is also found.

1. Introduction

Turbulent thermal convection in a horizontal heated layer of fluid has been of considerable interest in recent years. Turbulent motion first occurs when the Rayleigh number is increased by several orders of magnitude beyond the critical Rayleigh number for the initiation of convection. Malkus (1954*a*) presented a theoretical analysis of thermal convection together with his experimental findings (Malkus 1954*b*). One of the hypotheses in his analysis is that the heat transport due to turbulent thermal convection is maximized. Malkus's results describe fairly well the general behaviour of the fluid layer. The overall heat transfer Nusselt number is predicted to be proportional to the one-third power of the Rayleigh number at large Rayleigh numbers. Malkus's analysis also reflects his experimental observation of discrete heat flux transitions. The Nusselt number, instead of varying smoothly with the Rayleigh number, shows abrupt

slope changes (kinks) at certain Rayleigh numbers. The mean temperature distribution shows a boundary-layer-type structure: a nearly isothermal core with steep gradients close to the upper and lower bounding surfaces. Herring (1963, 1964), in a numerical study related to Malkus's work, found that under certain conditions the mean temperature in the central region of the layer can have a positive gradient, i.e. a gradient reversal exists in the layer. Herring attributes this gradient reversal to inadequacy of his mathematical model. The gradient reversal, although numerically small, is of some interest since one of the hypotheses of Malkus's theory is that the mean temperature gradient shall be non-positive throughout. Howard (1963) and more recently Busse (1969) calculated the upper bound of heat transport of thermal convection at large Rayleigh numbers. They both found that the Nusselt number varies as $Ra^{\frac{1}{2}}$ in the limit $Ra \to \infty$. Kraichnan (1962), using a mixing-length approach, found substantially the same dependence, $Nu \propto Ra^{\frac{1}{2}}/(\ln Ra)^{\frac{3}{2}}$. Busse's (1969) results also show kinks in the Nusselt–Rayleigh relation.

Deardorff (1965) numerically modelled thermal convection at a Rayleigh number of $6{\cdot}75 \times 10^5$ for an air layer as well as a fluid layer of Prandtl number 10. The temperature profile shows a slight gradient reversal for both Prandtl numbers. Again, the reversal is attributed to inadequacy of the model.

There are a number of measurements of the heat transfer through horizontal heated layers. The data generally show that the Nusselt number varies as the Rayleigh number raised to a power of one-third or slightly less. However, the accuracy of these results is such that the discrete transitions as observed by Malkus were not confirmed for nearly ten years. Recent measurements seem to show (Willis & Deardorff 1967; Rossby 1966) that discrete transition occurs at least up to a Rayleigh number of about 3×10^6, although there is still no unanimity on the subject.

Townsend (1959), Deardorff & Willis (1967*a*, *b*) and Goldstein & Chu (1969) made measurements of temperature profiles in air layers. The data of the latter two experiments show close agreement (Chu 1971). Reversed gradients are not noted in these experiments although one of Townsend's profiles shows a gradient reversal. Some of Sommerscales & Gazda's (1969) profiles in high Prandtl number fluids have abrupt gradient changes near the boundaries; the central region seems to be essentially isothermal.

With the large body of theoretical and experimental studies and their somewhat conflicting results, it is highly desirable to have accurate measurements against which the merits of various models could be compared. The present experimental study attempts to provide some of the measurements. The first part of the study contains overall heat flux measurements through heated water layers; the Rayleigh number ranges from $2{\cdot}76 \times 10^5$ to $1{\cdot}05 \times 10^8$. In the second part of the study, measurements of mean temperature profiles of thermal convection are made in a Rayleigh number range $3 \times 10^5 < Ra < 2 \times 10^7$. An interferometric method is used. Qualitative observations are also made of the general behaviour of the temperature field of thermal convection.

2. Apparatus and measurement technique

The test apparatus is built for both heat transfer and temperature distribution measurements. Heat transfer measurements are first made. Later, with some modifications, the test section is used for temperature distribution measurements.

Heat transfer measurements

The horizontal extent of the convection chamber is 15·24 × 25·40 cm. The sides of the chamber are made of 1·27 cm thick Plexiglas.

The fluid layer is heated from below by passing a d.c. current through a 0·0025 cm thick stainless-steel heating foil in direct contact with the layer. The foil is glued to a 3·18 cm thick Plexiglas base machined to a flatness of within 0·003 cm. Each opposite 15·24 cm end of the foil is soldered to a 0·025 cm copper sheet. Seven 6 mm tabs from each copper sheet are then soldered to solid copper bus bars. A seven-junction copper-constant thermopile measures the average temperature of the foil. The junctions are flush with the top surface of the base; they are insulated from the foil by a thin layer of epoxy glue.

The fluid layer is bounded above by a constant-temperature copper plate supported by 1·27 cm diameter precision-machined Plexiglas spacers, one at each of the four corners. The constant-temperature plate is made of a 2·54 cm thick copper plate 15·0 × 25·32 cm with eight 1·27 × 1·27 cm channels cut in the back for circulating water from a constant-temperature bath. The temperature of the circulating bath can be regulated to within 0·01 °C. The back of the plate is closed by a 0·90 cm thick brass plate. The plate temperature is measured by a seven-junction thermopile.

An identical constant-temperature plate is glued to the back of the heating-foil base to serve as a guard heater. To minimize heat conduction along the Plexiglas walls, 60 % of the wall area enclosing the fluid layer is machined down to a thickness of 3 mm; the material removed is replaced by urethane foam. The entire test section is then insulated on all sides by 5 cm thick urethane foam boards. The average of the top and bottom surface temperature is always close to the room temperature to reduce heat loss.

The electric power to the heating foil comes from two 4·5–9·0 V, 0–15 A d.c. power supplies operating in parallel for high-current output. The voltage output is regulated to within 0·3 %. Variable resistors in series with the heating foil are used to adjust the current flow: a precision shunt is used to measure the current. The resistance of the foil is measured by a precision bridge with an accuracy of 0·1 %, and found to be 0·05036 Ω at 23·5 °C. A temperature correction factor is applied for different operating temperatures. For each heat transfer measurement, values of the bounding surface temperatures and the current flow to the heating foil are obtained. The e.m.f. output of the heater thermopile is monitored for 30 to 60 min; the average of the extreme values is used in calculations. The peak-to-peak temperature fluctuation is about 5 % of the overall temperature difference. The temperature difference between the guard heater and the heating foil is typically less than 0·04 °C.

Mean temperature measurements

A Mach–Zender interferometer with a helium–neon laser source is used for temperature measurements. An interferometer actually measures the index-of-refraction field. Temperature is calculated from an equation of state relating the two properties (Tilton & Taylor 1938). For small temperature differences, the change of index of refraction is essentially proportional to the change of temperature.

The mean temperature profile is obtained by a time exposure technique which has been used successfully in Goldstein & Chu's (1969) study of thermal convection in air layers. The light beam of the interferometer integrates the temperature field spatially as it passes horizontally through the layer. A time exposure of the interference pattern results in a spatial–time mean of the fluctuating temperature field. Implicit in the method is the assumption that the time-averaged temperature at a fixed position is equivalent to the combined spatial–time average actually measured. Visual and photographic studies (*Thermal Convection Film*, University of Minnesota Heat Transfer Laboratory, 1972) are also made of the fluctuating instantaneous interferograms to infer the general behaviour of the temperature field. The instantaneous interferograms represent the one-dimensionally averaged temperature field.

Since the heating foil, acting somewhat as a constant-heat-flux surface (see below), produces significant temperature fluctuation at the lower surface, the resulting time-averaged interferograms are rather difficult to analyse. Therefore, for temperature distribution measurements the foil is discarded; the constant-temperature plate that previously served as the guard heater is used to heat the fluid from below. A fused silica optical window 5 cm in thickness and 15 cm in diameter is installed on each of the 25·4 cm sides of the test section. The windows are first fitted into aluminium frames; the frames are then bolted onto the Plexiglas side walls. Sealing between the frame and the side wall is provided by O-rings and silicone rubber sealant. Thus, the joints between the window frame and the side walls are slightly flexible. To prevent any tilting of the windows owing to the thermal expansion effects of the side walls, two $1{\cdot}25 \times 10$ cm aluminum plates spanning the test section above and below are bolted to the frames to keep them at a fixed distance apart. A schematic diagram of the test section is shown in figure 1.

Thirty-minute time exposures are used to obtain time–spatial average interferograms. Three to four time exposures are made for each experimental setting; a $\frac{1}{30}$s exposure precedes each time exposure as a record for comparison. A Canon FT, 35 mm camera with a 50 mm/f1·4 lens is used to record the interferograms on Panatomic-X films. The film is developed in Microdol-X developers for 12 min at 20 °C. Panatomic-X is chosen because of its fine grain structure.

In using the interferometer, two initial settings are possible. With infinite fringes (i.e. fringes very widely spaced), each fringe, once the experiment is underway, represents a contour of constant temperature (averaged along the light beam). With initially finite or wedge fringes (adjusted to be vertical in this experiment) the temperature change is proportional to the deviation from the initial vertical lines.

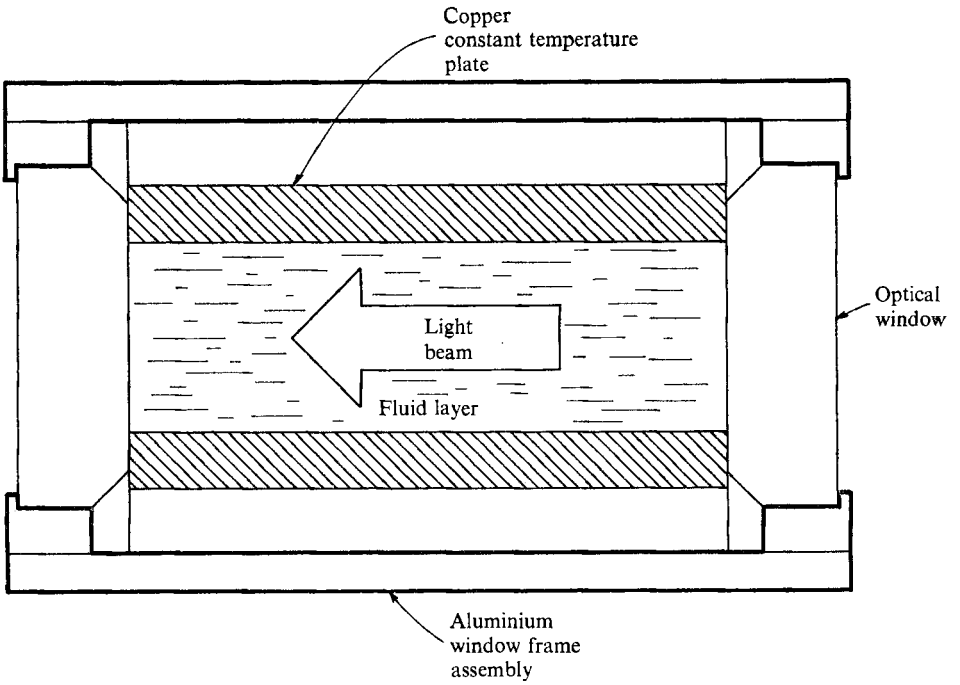

FIGURE 1. A schematic diagram of the test section.

3. Heat transfer through a horizontal water layer heated from below

Overall heat transfer measurements are made for four layer depths. The Rayleigh number ranges from $2{\cdot}76 \times 10^5$ to $1{\cdot}05 \times 10^8$. A total of fifty data points are taken. The range of data taken is summarized in table 1.

The heat transfer data are correlated in terms of Nusselt and Rayleigh numbers:

$$Nu = hD/k, \quad Ra = g\beta\Delta T D^3/\nu\alpha,$$

where k is thermal conductivity, β is the coefficient of thermal expansion, g is the gravitational acceleration, ν the kinematic viscosity and α the thermal diffusivity. The thermophysical properties are evaluated at the average of the two surface temperatures, which, in fact, is the mid-plane temperature. D and ΔT are respectively the layer depth and the temperature difference; h is the heat transfer coefficient based on ΔT.

A correlation of the form

$$Nu = \text{constant} \times Ra^n$$

is assumed. Since water is the only fluid used in the experiment, the range of Prandtl number is very small (5·45–6·50). It is not included in the correlation. The resulting heat transfer correlation is

$$Nu = 0{\cdot}183(Ra)^{0{\cdot}278}, \quad 2{\cdot}76 \times 10^5 < Ra < 1{\cdot}05 \times 10^8.$$

The correlation is obtained by a linear regression of $\ln(Nu)$ versus $\ln(Ra)$ through 50 data points. The standard error of the regression coefficient is 0·001.

Layer depth D (cm)	Temperature difference Δt (°C)	Aspect ratio L/D	Rayleigh number $Ra = g\beta\Delta TD^3/\nu\alpha$
2·53	0·99–5·04	6·02	$2{\cdot}76-10^5$–$1{\cdot}13\times10^6$
3·80	0·50–4·09	4·02	$4{\cdot}91\times10^5$–$3{\cdot}87\times10^6$
6·34	1·07–4·23	2·40	$4{\cdot}65\times10^6$–$1{\cdot}86\times10^7$
10·16	0·86–3·99	1·50	$2{\cdot}27\times10^7$–$1{\cdot}05\times10^8$

TABLE 1. Aspect ratio is defined as the ratio of the width of the test section (15·24 cm) and the layer depth; the horizontal extend of the test section is 15·24 × 25·40 cm

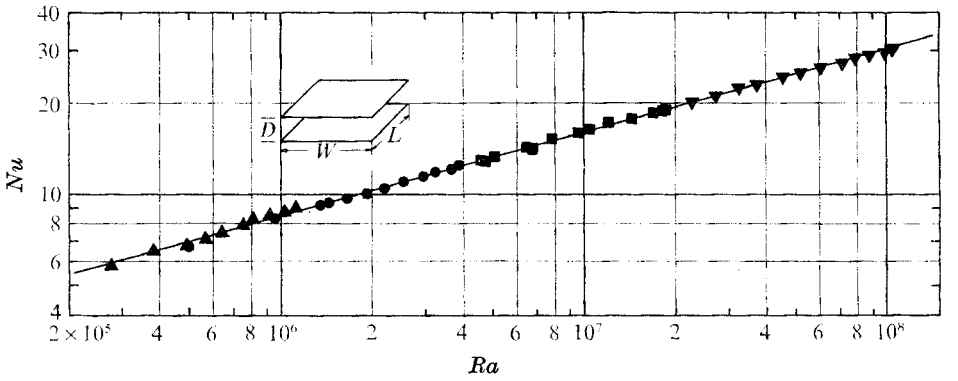

FIGURE 2. Overall heat transfer correlation. $2{\cdot}76\times10^5 < Ra < 1{\cdot}05\times10^8$; W = 25·40 cm, L = 15·24 cm. ——, $Nu = 0{\cdot}183Ra^{0{\cdot}278}$; ▲, D = 2·53 cm, L/D = 6·02; ●, D = 3·80 cm, L/D = 4·02; ■, D = 6·34 cm, L/D = 2·40; ▼, D = 10·16 cm, L/D = 1·50.

The correlation coefficient is 0·99955. The maximum deviation of any data point from the fit is 4·27 %. The root-mean-square deviation of all the data from the fit is 1·4 %. Figure 2 shows the data points and the correlation. As in all recent experiments (Garon 1970; Goldstein & Chu 1969; Rossby 1966), the dependence of the Nusselt number on the Rayleigh number is less than the one-third power. Figure 3 is a comparison of the present correlation with the data taken in water layers by Rossby (1966), Silveston (1958), Globe & Dropkin (1959) and Garon (1970). The present experiment shows close agreement with the data of Rossby and Silveston and most of the data of Globe & Dropkin. The agreement between Garon's data and the present experiment is within 5 % at a Rayleigh number of 2×10^7; the agreement improves to within 4·7 % at a Rayleigh number of 10^8. Also shown in figure 3 is the correlation by O'Toole & Silveston (1961) based on available data up to 1960. This correlation is within 10 % of the present one.

There has been no experimental verification of discrete transitions over the entire present Rayleigh number range. To test for possible existence of these transitions, linear plots of $RaNu$ versus Ra are made. Eight transitions are found. They occur at Rayleigh numbers of $6{\cdot}10\times10^5$, $1{\cdot}63\times10^6$, $2{\cdot}65\times10^6$, $5{\cdot}80\times10^6$, $1{\cdot}06\times10^7$, $2{\cdot}05\times10^7$, $4{\cdot}10\times10^7$ and $7{\cdot}00\times10^7$. These values are obtained using a single plate spacing or data overlapping on both sides of the transition from two plate spacings except for the transition at $2{\cdot}05\times10^7$.

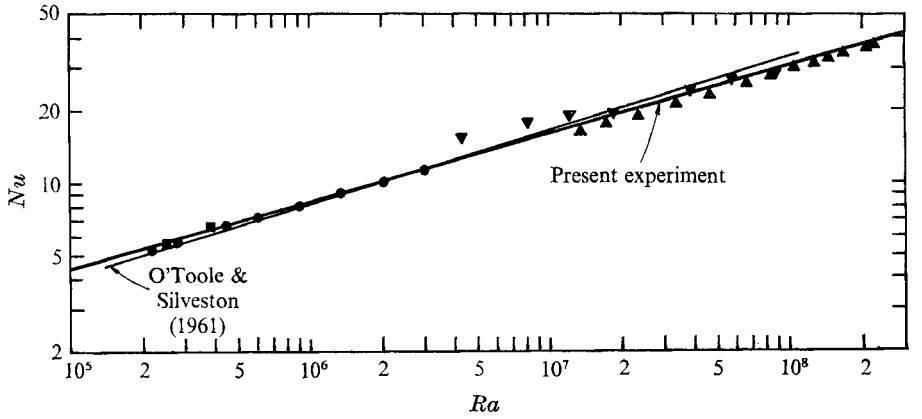

FIGURE 3. Comparison of present correlation with previous experimental data. ●, Rossby (1966); ■, Silveston (1958); ▼, Globe & Dropkin (1959); ▲, Garon (1970).

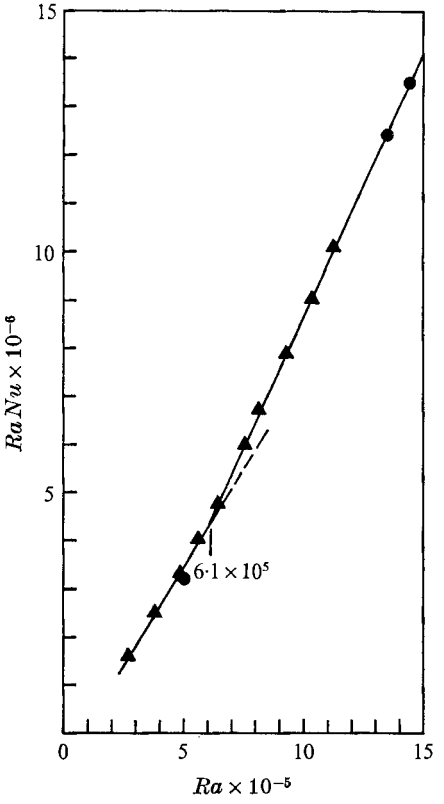

FIGURE 4. A point of discrete heat flux transition. ▲, D = 2·53 cm; ●, D = 3·80 cm.

Figure 4 is an example of a transition with overlapping data from two spacings. Figure 5 summarizes all the experimental transitional points together with the transitional Rayleigh numbers from the linear stability calculations of Catton (1966) in the range of the present study. There is a lack of agreement among the different experiments and between any of the experiments and the calculations

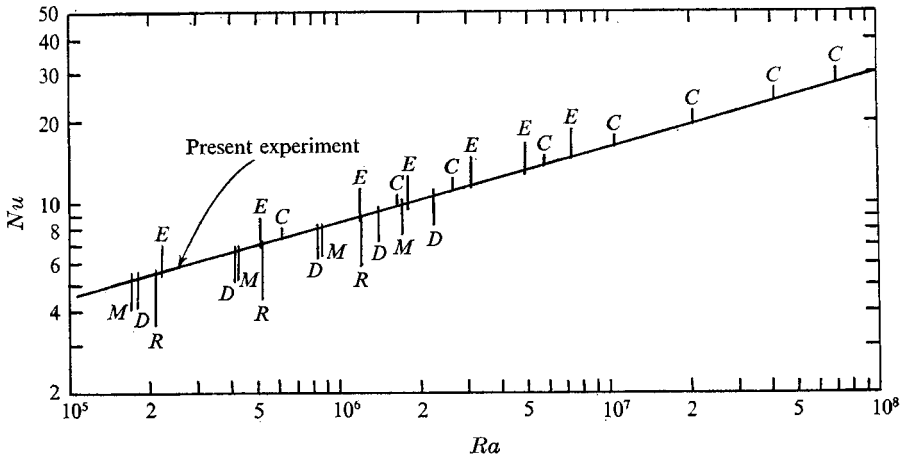

FIGURE 5. A summary of points of discrete transition. *E*, Catton (1966) (calculation); *M*, Malkus (1954*b*); *D*, Deardorff (1965); *R*, Rossby (1966); *C*, present experiment.

of Catton. Part of the difficulty is the extreme accuracy required of the data to pinpoint the transitions. The variation of fluid properties with temperature, the exact thermal boundary condition and the test-section geometry may also have some influence. In both Malkus's theory and Catton's calculation, the transitional Rayleigh numbers are independent of the Prandtl number. This is possibly incorrect. For example, the transition from laminar to turbulent thermal convection has been shown to be a rather strong function of the Prandtl number. Despite all the disagreements, the present data, together with previous experiments, appear to confirm the presence of transitions. If one looks at each set of experiments individually, the relative positions of the transitions are approximately the same. With the present state of theories and experiments, this qualitative agreement is perhaps the most one should expect.

Some question arises as to the nature of the thermal boundary conditions at the foil's heated lower surface. Although this was originally intended to serve as a constant-heat-flux boundary condition, measurement of the critical Rayleigh number for the onset of flow gives a value of 1534, in between the theoretical values of 1296 (Sparrow, Goldstein & Jonsson 1964) for constant-heat-flux and 1708 for constant-temperature boundary conditions at the bottom boundary with constant temperature at the upper boundary. As in many heat transfer problems, the effect of the thermal boundary conditions on the results is expected to be less important when the flow becomes turbulent. This is borne out by the agreement between the measured heat transfer with the two different bottom plates used in this experiment (cf. § 5).

4. A qualitative description of the thermal convection temperature field

A qualitative general description of the thermal convection temperature field, determined from visual and photographic observations of the interferogram patterns as a function of time, is given in this section. An instantaneous interferogram actually represents a one-dimensionally averaged temperature field

at a particular moment; despite this limitation, the observations yield some informative insight into the mechanism of thermal convection.

At low Rayleigh numbers, the temperature field shows a steady periodic laminar pattern. Figure 6(*b*) (plate 1) is an example of the regular pattern at a Rayleigh number of $9{\cdot}6 \times 10^3$. The spatial periodicity of the pattern is about $2D$. Figure 6(*a*) (plate 1) is the convection pattern in air at a similar Rayleigh number ($7{\cdot}0 \times 10^3$). The interferograms are taken with infinite-fringe adjustment. The lines are essentially isotherms. One major difference between the two patterns is the shape of the central isotherm. In the water layer, the central isotherm doubles back. This doubling back of the central isotherm indicates local gradient reversal in the averaged temperature field. Figures 7(*a*) and (*b*) (plate 1) show the convection pattern at a Rayleigh number of $3{\cdot}15 \times 10^4$ at two different instants. The temperature field is not quite steady at this Rayleigh number. The spatial periodicity changes slightly with time; however, the pattern is still essentially regular. Since the pattern represents a spatial average, it is not clear how to distinguish cells from rolls. Nevertheless, the patterns show close resemblance to Veronis's (1966) two-dimensional roll calculations.

As the Rayleigh number is increased, the regular structure breaks down; the flow becomes turbulent. The turbulent thermal convection temperature field is characterized by a boundary-layer structure with steep gradient near each bounding surface and a 'nearly isothermal' core in the central region. The main heat transfer mechanism near the wall is the release of thermals from the edge of the boundary layers. A thermal is a mass of fluid, driven by buoyancy, that moves away from a bounding surface into the bulk of the fluid layer. In the fluid layer, there are actually warm thermals from the bottom surface and cold thermals from the top surfaces. For the purpose of the present discussion, Rayleigh numbers up to 5×10^5 will be termed moderate. Those over 5×10^6 will be termed high. At moderate Rayleigh numbers thermals, after bursting out from the boundary layer, travel vertically through the central core rather quickly ('quickly' will become better defined later). Even though the interferometer gives an 'average' view of the temperature field, thermals are often seen. The number observed might be larger if some were not washed out by the integration that the light beam performs.

Many of the thermals still retain some of their original identity, temperature difference, when they reach the vicinity of the other surface. The remains of these far-reaching thermals tend to coalesce to form masses of relatively warm fluid near the top surface and masses of relatively cold fluid near the bottom surface. These masses of fluid will be referred to as 'stable blobs' since they are stable with respect to the central core. These 'stable blobs' persist for rather long periods of time (as compared with the time required for a thermal to travel through the central core) before losing their identity. Let δ be the typical dimension of the boundary layer. 'Stable blobs' are observed to be typically δ–2δ in thickness and 2δ–5δ in width; some of them are as large as 10δ in width. Thermals are released at 'relatively fixed sites' over short periods of time. 'Relatively fixed sites' means that several successive thermals may come from approximately the same location on a surface. However, over a long period of observation, there do

not seem to be any fixed or preferred sites. Figure 8 (plate 2) shows the release of a thermal from the warm bottom boundary layer. Near the root of the thermal, one can also see one of the 'stable blobs'. Coexisting with the active thermal release regions are regions of fluctuation characterized by moving fronts of warm or cold fluid. These moving fronts have a temperature only slightly different from the surroundings. Their movements show up as moving ripples through the essentially vertical (isothermal) finite fringes. At any one instant there are fronts moving in both directions. Figure 9 (plate 3) shows the ripples.

From the above description, one obtains a qualitative picture of the temperature fluctuation in the layer at moderate Rayleigh numbers. At the wall the temperature fluctuation is zero (isothermal walls). The fluctuation increases to a maximum at the edge of the boundary layer, where the thermals are released. This fluctuation is characterized by the alternating periods of large amplitude active thermal release and small amplitude fluctuations. The active period tends to persist for a short time because thermals are released at relatively fixed sites. With increasing height beyond the boundary layer, the frequency of occurrence of active periods decreases since some thermals are dissipated before reaching the central region of the layer. At moderate Rayleigh numbers (up to 5×10^5), because of the relatively large number of 'stable blobs', the average temperature outside the bottom boundary layer is lower than that of the mid-plane and the temperature outside the top boundary layer is higher than the mid-plane temperature. The temperature decreases sharply away from the bottom wall. Beyond the bottom boundary layer, the gradient reverses; temperature increases slightly with height until the vicinity of the top boundary layer, where temperature again decreases sharply with height.

As the Rayleigh number is further increased to about 5×10^6, a persistent horizontal motion is observed near the horizontal boundaries. This motion might be a result of the unfavourable aspect ratio ($L/D = 1{\cdot}2, 1{\cdot}5$); however, this change of character of flow was also observed by Malkus (1954*b*) in acetone. Instead of rising vertically after maturing, the thermals travel horizontally for a distance of the order of the layer depth before breaking away from the boundary layer. Figure 10 (plate 4) shows the horizontal movement of a thermal after breaking away from the boundary layer. The horizontal movement of a thermal persists until it is about 10δ away from the boundary. Beyond 10δ the thermal travels essentially vertically. The population of 'stable blobs' decreases rapidly with increasing Rayleigh number because of the mixing effect of the horizontal motion. At high Rayleigh numbers (5×10^6), 'stable blobs' are observed only rarely. Because of the persistent horizontal movement of the thermals, the temperature fluctuation near the boundary becomes more regular. The active periods are then expected to be more regularly spaced (in time). Occasionally there will be an extremely active period corresponding to the bursting away of a thermal. As at moderate Rayleigh numbers, away from the wall the active periods occur less frequently. Near the mid-plane temperature fluctuation is almost solely characterized by the moving ripples (figure 9). At high Rayleigh numbers the average temperature distribution has an isothermal central region.

For moderate-to-high Rayleigh numbers ($5 \times 10^5 < Ra < 5 \times 10^6$) the

Layer depth D (cm)	Temperature difference ΔT (°C)	Aspect ratio L/D	Rayleigh number Ra
3·80	0·311–0·441	4·02	$3{\cdot}11\times10^5$–$3{\cdot}97\times10^5$
6·34	0·164–0·380	2·40	$8{\cdot}01\times10^5$–$1{\cdot}72\times10^6$
10·16	0·297–0·463	1·50	$5{\cdot}88\times10^6$–$9{\cdot}34\times10^6$
12·70	0·310–0·455	1·20	$1{\cdot}27\times10^7$–$1{\cdot}86\times10^7$

TABLE 2. L = 15·24 cm (L is along the light beam direction). The horizontal extent of the test section is 15·24 × 25·4 cm

temperature field shows characteristics of both moderate and high Rayleigh numbers. The horizontal movement of thermals and the existence of 'stable blobs' are both observed.

5. The mean temperature distribution of thermal convection

Average temperature distribution measurements are obtained from time-averaged interferograms for four depths: 3·80, 6·34, 10·16 and 12·70 cm. The first and second spacings correspond respectively to moderate and moderate-to-high Rayleigh number ranges. The last two spacings correspond to high Rayleigh numbers. The temperature difference across the fluid layer is typically 0·15–0·50 °C. For the two smaller spacings, profiles are measured from both boundaries. For large spacings, because of the limited field of view of the interferometer, measurements are only made from the bottom wall. The range of data taken is summarized in table 2.

The mean temperature distributions are presented in dimensionless form. The dimensionless temperature θ is the magnitude of the temperature, $T_Z - T_m$, normalized by half the temperature difference, $\frac{1}{2}\Delta T$, across the layer:

$$\theta = |T_Z - T_m| / \tfrac{1}{2}\Delta T.$$

Z and m denote conditions at a distance Z from the bounding surface and at the mid-plane respectively. The dimensionless length η is the ratio of Z and the boundary-layer thickness δ, which is the subtangent of the temperature distribution curve. It can easily be shown that δ is equal to $D/2Nu$. In θ, η co-ordinates, the wall gradient is always -1. For certain presentations Z is also made dimensionless by the layer thickness D.

The mean temperature field at moderate Rayleigh number is characterized by a gradient reversal in the central region of the layer. As discussed in the last section, the reversal is caused by relatively large number of 'stable blobs' near the bounding surfaces. Figure 11 (plate 5) is a time-averaged interferogram with a gradient reversal.

Figure 12 shows a typical mean temperature profile with a gradient reversal. The overall profile is symmetric, within experimental accuracy. Three mean temperature profiles are obtained for moderate Rayleigh numbers. They are presented in θ, η co-ordinates in figure 13. Only the bottom wall to the mid-plane

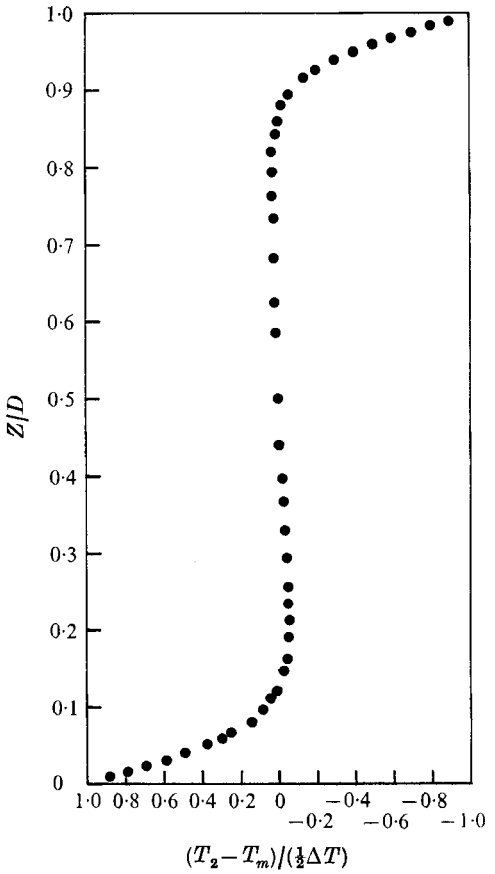

FIGURE 12. A typical mean temperature profile in a water layer with a gradient reversal. $Ra = 3{\cdot}97 \times 10^6$, $D = 3{\cdot}80$ cm, $\Delta T = 0{\cdot}441$ °C.

part of the profiles are plotted as the profiles are symmetric. θ decreases away from the wall; it reaches 0 at $\eta = 1{\cdot}75$. θ continues to drop beyond 1·75. The minimum of θ occurs at about 2·6. The average maximum overshoot of temperature (absolute value of the minimum of θ) is about 0·04.

Previous experiments (Sommerscales & Dropkin 1966; Townsend 1959) have found reversed gradients in thermal convection. They have been attributed to experimental errors. Sommerscales & Gazda (1969) in a more recent experiment observed gradient reversals in high Prandtl number fluids for Rayleigh numbers ranging from $7{\cdot}39 \times 10^5$ to $1{\cdot}47 \times 10^7$. Their profiles are quite asymmetric; the reversals do not always occur at both boundaries. They assume that gradient reversal is related to the appearance of long period fluctuations in the fluid layer. The value of the maximum overshoot found by Sommerscales & Gazda shows up as abrupt kinks outside of the boundary layer; the interior of the layer seems almost isothermal. On the other hand, the profile of the present experiment shows a smooth and gradual change throughout the layer. The gradient reversal predicted theoretically by Herring (1964) is also confined to two peaks at the edge of

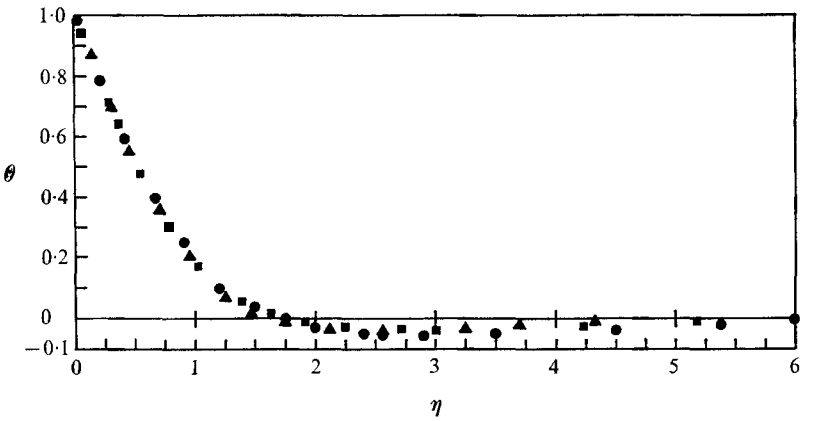

FIGURE 13. Dimensionless mean temperature profiles with gradient reversal in a water layer; $3{\cdot}11 \times 10^5 < Ra < 3{\cdot}95 \times 10^5$, $D = 3{\cdot}80$ cm. ▲, $Ra = 3{\cdot}11 \times 10^5$, $\Delta T = 0{\cdot}311$ °C; ■, $Ra = 3{\cdot}65 \times 10^5$, $\Delta T = 0{\cdot}383$ °C; ●, $Ra = 3{\cdot}97 \times 10^5$, $\Delta T = 0{\cdot}441$.

the boundary layer rather than the smooth transition observed in the present experiment.

Goldstein & Chu (1969) and Deardorff & Willis (1967*a*, *b*) have made extensive measurements of mean temperature profiles in air. The lowest Rayleigh number in both experiments is about 6×10^5. Neither experiment finds any gradient reversal. However, a re-examination of some of the motion pictures taken by Goldstein & Chu at a Rayleigh number of 2×10^5 indicates reversed gradients. Rossby (1966) has found that the Rayleigh number for the onset of time-dependent motion in fluid layer varies approximately as $Pr^{0{\cdot}6}$. Therefore, an air layer would become turbulent at a Rayleigh number approximately four times lower than that for a water layer. Since a reversed gradient for turbulent thermal convection occurs only at relatively low Rayleigh numbers, one could expect to observe gradient reversal at a lower Rayleigh number in air than in water.

No special effort has been made to examine the lower and upper limits of the occurrence of gradient reversal. However, from the data taken for the present experiment and subsequent observations made during the motion picture studies, it was found that gradient reversal existed at least up to $Ra = 4{\cdot}8 \times 10^5$. There is reason to believe that gradient reversal may occur even up to a Rayleigh number of 6×10^5 (Chu 1971). As for the lower limit of gradient reversal, laminar pattern observations in water (not in air, see figure 6) show that a reversed mean temperature gradient may be present at quite low Rayleigh numbers.

As the Rayleigh number is further increased, more and more thermals are dissipated before reaching the opposite surface; the reversed gradient disappears. With increasing Rayleigh number, the dimensionless temperature profile shows progressively more gradual variation away from the bounding surface. Figure 14 shows the change of the profile with Rayleigh number. The profile at $8{\cdot}01 \times 10^5$ probably represents the last stage of the evolution from a positive to negative temperature gradient outside the boundary layer.

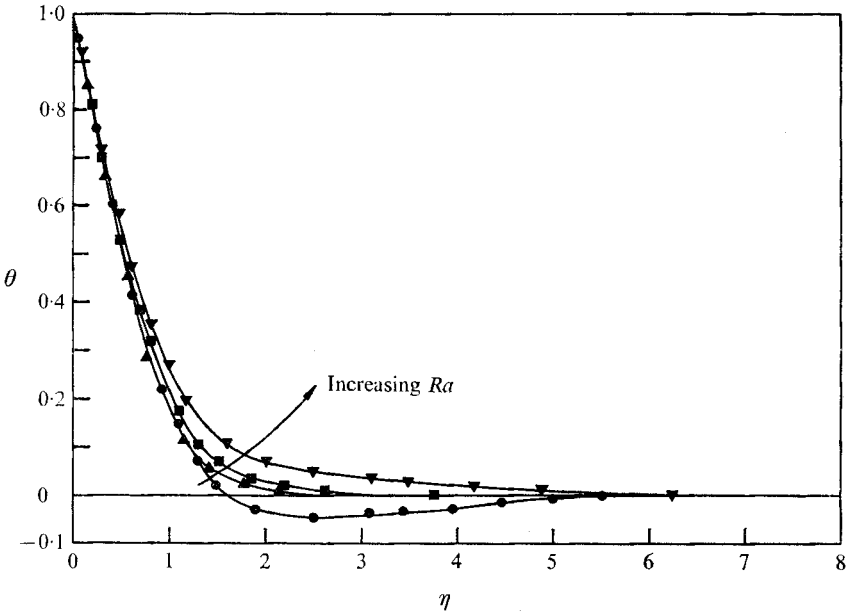

FIGURE 14. Variation of dimensionless mean temperature profiles in a water layer with Rayleigh number. ●, $Ra = 3{\cdot}11 \times 10^5$; ▲, $Ra = 8{\cdot}01 \times 10^5$; ■, $Ra = 1{\cdot}72 \times 10^6$; ▼, $Ra = 1{\cdot}56 \times 10^7$.

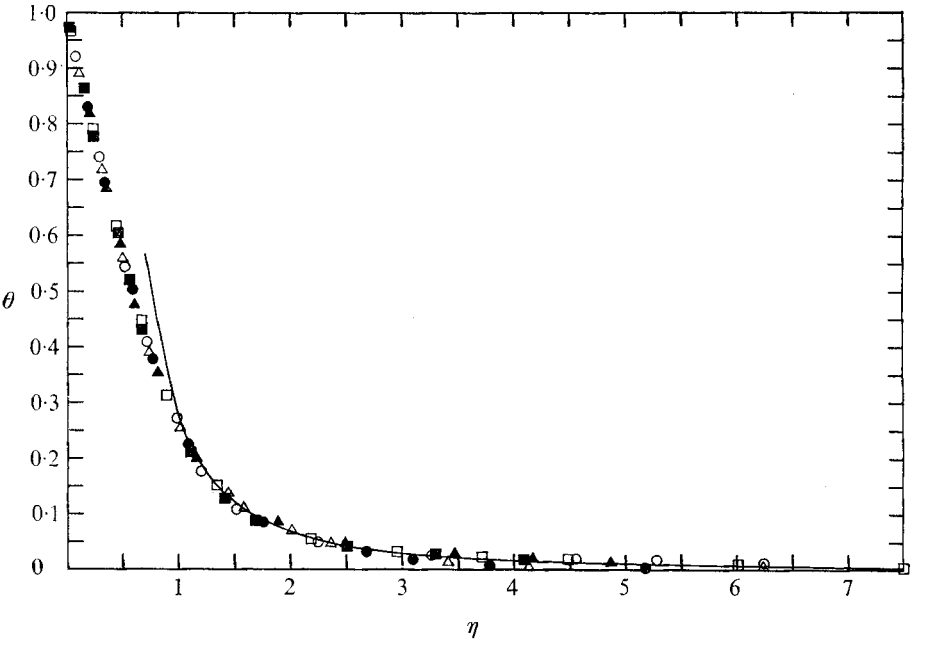

FIGURE 15. Dimensionless temperature distribution for high Rayleigh numbers ($5{\cdot}88 \times 10^6 < Ra < 1{\cdot}86 \times 10^7$) with the best-fit power law, $\theta = 0{\cdot}275\eta^{-2}$ (solid line).

	○	△	□	●	▲	■
Ra	$5{\cdot}88 \times 10^6$	$7{\cdot}09 \times 10^6$	$9{\cdot}34 \times 10^6$	$1{\cdot}28 \times 10^7$	$1{\cdot}56 \times 10^7$	$1{\cdot}86 \times 10^7$
D (cm)	10·16	10·16	10·16	12·70	12·70	12·70
ΔT (°C)	0·297	0·366	0·463	0·310	0·382	0·455

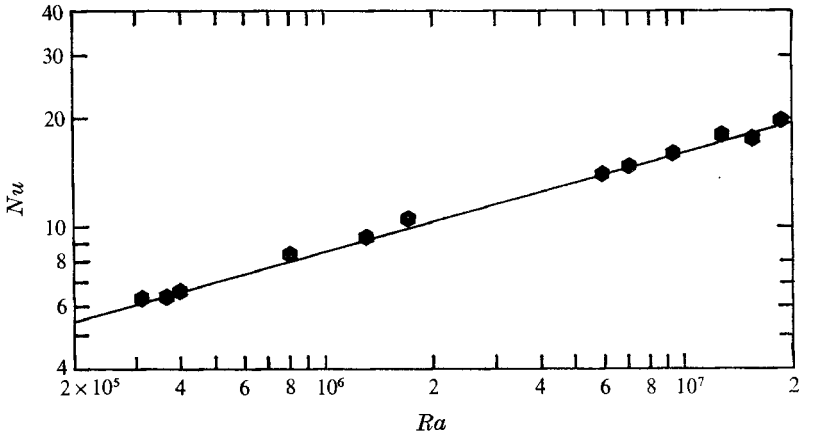

FIGURE 16. Heat transfer results from temperature distribution measurements. ——, $Nu = 0{\cdot}183\ Ra^{0{\cdot}278}$; ●, fringe data.

Six mean temperature profiles are obtained for Rayleigh numbers above the transition from positive to negative central gradient: three each for layer depths of 10·16 cm and 12·70 cm. The Rayleigh number ranges from $5{\cdot}88 \times 10^6$ to $1{\cdot}86 \times 10^7$. All profiles follow essentially the same trend as that shown in figure 15.

Nusselt numbers are calculated from the wall gradients for all the temperature profiles. The results are in good agreement with the heat transfer correlation, as shown in figure 16. The root-mean-square deviation from the correlation is 3·3 %.

According to Malkus's (1954*a*) analysis, the variation of temperature away from the surface should follow a Z^{-1} power law. In θ, η co-ordinates, this power law can be expressed as

$$\theta = (2/\pi^2)\,\eta^{-1}, \quad \eta > 1/\pi\ (= 0{\cdot}32).$$

Kraichnan's analysis also predicts a Z^{-1} power law; he also found a $Z^{-\frac{1}{2}}$ law further into the interior of the layer.

The temperature distributions for each Rayleigh number range are plotted in $\partial\theta/\partial\eta$, η co-ordinates with logarithmic scales to check possible power-law dependence of θ on Z ($\sim \eta$). Figure 17 shows some of these distributions. A Z^{-n} power law would yield a slope of $-(n+1)$ on the $\partial\theta/\partial\eta$ *vs.* η graph. Plotting temperature profiles in $\partial\theta/\partial\eta$, η co-ordinates has certain advantages. In many experiments, the measured mid-plane temperature is not equal to the average of the wall temperatures. This difference is either due to large property variations (Rossby 1966) or long period, local temperature drift (Sommerscales & Gazda 1969). A $\partial\theta/\partial\eta$ *vs.* η plot eliminates the effect of the mid-plane temperature. Also, frequently, when examining data for power-law dependence, there is a tendency to draw a chord rather than a tangent through the data points. The $\partial\theta/\partial\eta$ *vs.* η plot is a good check against such a mistake.

A $Z^{-\frac{1}{2}}$ law cannot be fitted to any significant portion of the data. Malkus's Z^{-1} power law can be fitted to a small range of data, $0{\cdot}4 < \eta < 1{\cdot}0$ for all Rayleigh numbers investigated. The same limited agreement with Malkus' prediction has

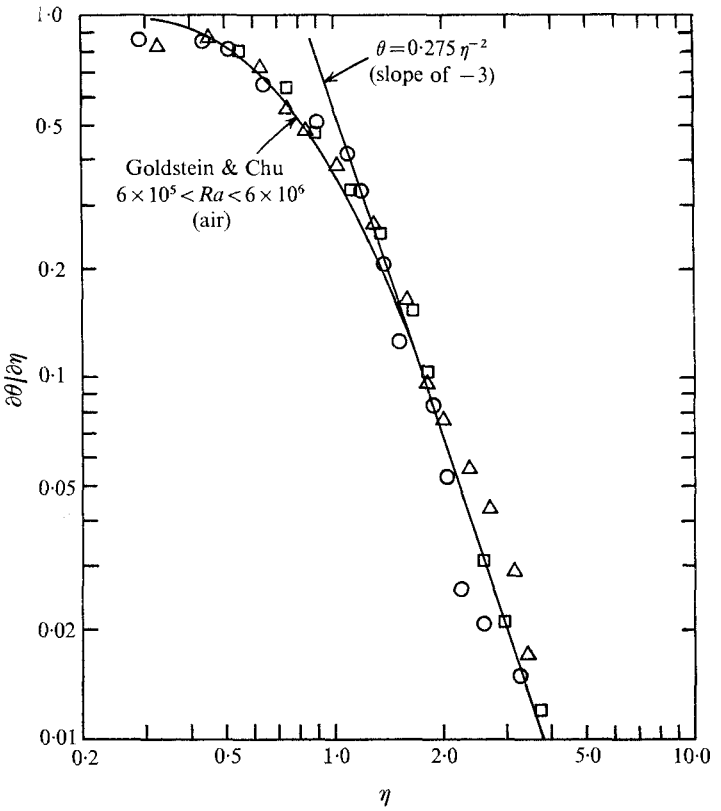

FIGURE 17. Log–log plot for power-law evaluation. D = 10·16 cm. ○, $Ra = 5{\cdot}88\times10^6$; △, $Ra = 7{\cdot}09\times10^6$; □, $Ra = 9{\cdot}34\times10^6$.

also been found in air for $6\times10^5 < Ra < 6\times10^6$ by Goldstein & Chu (1969). However, profiles for moderate to high Rayleigh numbers,

$$8{\cdot}01\times10^5 < Ra < 1{\cdot}76\times10^6,$$

show a possible power-law variation of $\theta \propto Z^{-3}$ in the range $1 < \eta < 3$. Sommerscales & Gazda (1969) reported similar findings for silicone oil (Pr = 6·18) in the Rayleigh number range 7×10^5–3×10^8.

The high Rayleigh number profiles ($5{\cdot}88\times10^6 < Ra < 1{\cdot}86\times10^7$) show agreement with a $\theta \propto Z^{-2}$ power law over a considerable range, $1 < \eta < 5{\cdot}5$ as shown in figures 15 and 17. The best fit is found to be

$$\theta = 0{\cdot}275\eta^{-2}.$$

A faired curve through the data of Goldstein & Chu for air for Rayleigh numbers between 6×10^5 and 6×10^6 is also plotted for comparison on figure 15. The two sets of data show excellent agreement for $\eta > 1$. Figure 18 compares the temperature profiles in water and air on linear scales. Again the profiles in water at a given Rayleigh number show agreement with profiles in air at a lower Rayleigh number. The agreement reflects a probable Prandtl number effect.

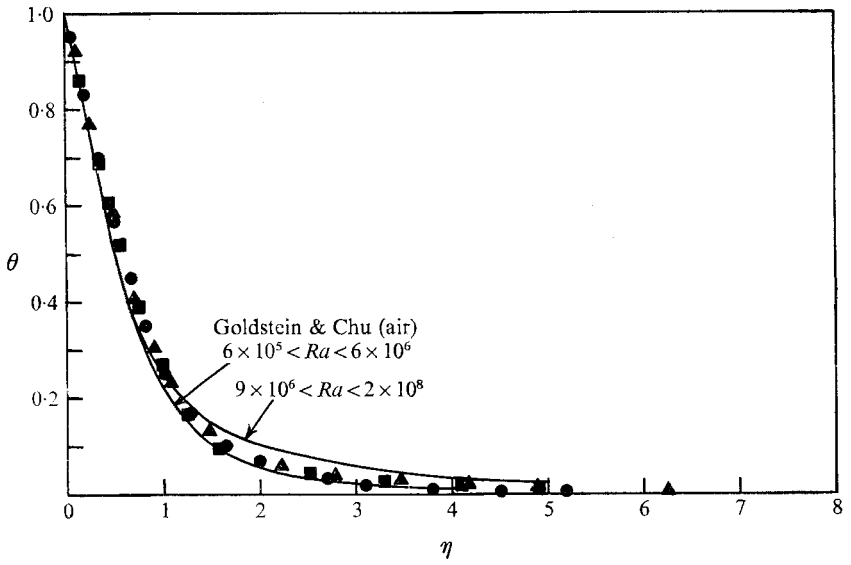

FIGURE 18. Comparison of thermal convection temperature profiles in air and water. Water data: ●, $Ra = 1{\cdot}28 \times 10^7$, $\Delta T = 0{\cdot}310$ °C, $Nu = 17{\cdot}91$; ▲, $Ra = 1{\cdot}56 \times 10^7$, $Nu = 17{\cdot}45$; ■, $Ra = 1{\cdot}86 \times 10^7$, $\Delta T = 0{\cdot}455$ °C, $Nu = 19{\cdot}71$. $D = 12{\cdot}70$ cm (mid-plane at $\eta = Nu$).

The present data show a decreasing power-law exponent (Z^{-3} is replaced by Z^{-2}) with increasing Rayleigh number. It is conceivable that eventually a Z^{-1} law could be approached at higher Rayleigh number as was found in air at $Ra \sim 10^8$.

6. Conclusion

Heat transfer measurements of turbulent thermal convection in horizontal water layers between Rayleigh numbers of $2{\cdot}76 \times 10^5$ and $1{\cdot}05 \times 10^8$ result in a correlation of the form

$$Nu = 0{\cdot}183 Ra^{0{\cdot}278}.$$

Eight discrete heat flux transitions are found in this Rayleigh number range. Comparison of published transition data and the present work indicates qualitative agreements among various experiments. The relative positions of the transitions appear to be approximately the same.

Interferometric observations show that a key heat transfer mechanism of turbulent thermal convection is the release of thermals from the boundary layers. At low Rayleigh numbers, remains of far-reaching thermals coalesce on opposite bounding surfaces to form 'stable blobs'. The 'stable blobs' cause a gradient reversal of the mean temperature distribution in the central region of the layer. As the Rayleigh number is increased, the thermals show a persistent horizontal movement near the bounding surfaces and the majority of the thermals are dissipated without reaching the opposite surface; the central region of the layer

becomes an isothermal core. One of the major findings of the present experiment is the fact that the movements of thermals have a direct bearing on the mean temperature distribution.

Mean temperature distributions are obtained by the time-averaging interferometry method. The dimensionless temperature distribution shows only a very limited agreement with the Z^{-1} power law. However, the distribution fits a Z^{-3} power law for moderate to high Rayleigh numbers, $Ra \sim 10^5$–10^6. For high Rayleigh numbers, $Ra \sim 10^6$–10^7, a considerable range of the distribution follows a Z^{-2} power law. It is conceivable that the trend is toward a Z^{-1} law with increasing Rayleigh number.

The authors gratefully acknowledge the support of the National Science Foundation (Grant GK-15252).

REFERENCES

Busse, F. H. 1969 On Howard's upper bound for heat transport by turbulent convection. *J. Fluid Mech.* **37**, 457.

Catton, I. 1966 Natural convection in horizontal fluid layers. *Phys. Fluids*, **9**, 2521.

Catton, I. & Edwards, D. K. 1967 Effect of side walls on natural convection between horizontal plates heated from below. *J. Heat Transfer*, **89**, 295.

Chu, T. Y. 1971 Thermal convection in horizontal liquid layers. Ph.D. thesis, University of Minnesota.

Deardorff, J. W. 1965 A numerical study of pseudo three-dimensional parallel-plate convection. *J. Atmos. Sci.* **22**, 419.

Deardorff, J. W. & Willis, G. E. 1967*a* Investigation of turbulent convection between horizontal plates. *J. Fluid Mech.* **28**, 675.

Deardorff, J. W. & Willis, G. E. 1967*b* The free-convection temperature profile. *Quart. J. Roy. Met. Soc.* **93**, 166.

Garon, A. 1970 Velocity measurements in turbulent thermal convection using a laser-doppler technique. Ph.D. thesis, University of Minnesota.

Globe, S. & Dropkin, D. 1959 Natural convection heat transfer in liquids confined by two horizontal plates and heated from below. *J. Heat Transfer*, **81**, 24.

Goldstein, R. J. & Chu, T. Y. 1969 Thermal convection in a horizontal layer of air. *Prog. Heat & Mass Transfer*, **2**, 55.

Herring, J. R. 1963 Investigation of problems in thermal convection. *J. Atmos. Sci.* **20**, 325.

Herring, J. R. 1964 Investigation of problems in thermal convection: rigid boundaries. *J. Atmos. Sci.* **21**, 227.

Howard, L. N. 1963 Heat transport by turbulent convection. *J. Fluid Mech.* **17**, 405.

Kraichnan, R. J. 1962 Mixing-length analysis of turbulent thermal convection at arbitrary Prandtl numbers. *Phys. Fluids*, **5**, 1374.

Malkus, W. V. R. 1954*a* Discrete transitions in turbulent convection. *Proc. Roy. Soc.* A **225**, 185.

Malkus, W. V. R. 1954*b* The heat transfer and spectrum of thermal turbulence. *Proc. Roy. Soc.* A **225**, 196.

O'Toole, J. L. & Silveston, P. L. 1961 Correlation of convective heat transfer in confined horizontal layers. *Chem. Engng Progr. Symp.* **32** (ser. 57), 81.

Rossby, H. T. 1966 An experimental study of Bénard convection with and without rotation. *Dept. Geol. Geophys. M.I.T. Sci. Rep.* HRF/SR27.

Silveston, P. L. 1958 Wärmedurchgang in Waagrechten Flüssigkeiksschichten. *Forsch. Ing, Wes.* **24**, 29.

SOMMERSCALES, E. F. C. & DROPKIN, D. 1966 Experimental investigation of the temperature distribution in a horizontal layer of fluid heated from below. *Int. J. Heat Mass Transfer*, **9**, 1189.

SOMMERSCALES, E. F. C. & GAZDA, I. W. 1969 Thermal convection in high Prandtl number liquids at high Rayleigh numbers. *Int. J. Heat Mass Transfer*, **12**, 1491.

SPARROW, E. M., GOLDSTEIN, R. J. & JANSSON, V. 1964 Thermal instability in a horizontal fluid layer; effect of boundary conditions and non-linear temperature profile. *J. Fluid Mech.* **18**, 513.

TILTON, L. W. & TAYLOR, J. K. 1938 Refractive index and dispersion of distilled water for visible radiation, at temperatures 0 to 60 °C. *Nat. Bur. Stand. J. Res.* **20**, 419.

TOWNSEND, A. A. 1959 Temperature fluctuations over a heated surface. *J. Fluid Mech.* **5**, 209.

VERONIS, G. 1966 Large-amplitude Bénard convection. *J. Fluid Mech.* **26**, 49.

WILLIS, G. E. & DEARDORFF, J. W. 1967 Confirmation and renumbering of the discrete heat flux transitions or Malkus. *Phys. Fluids*, **10**, 1861.

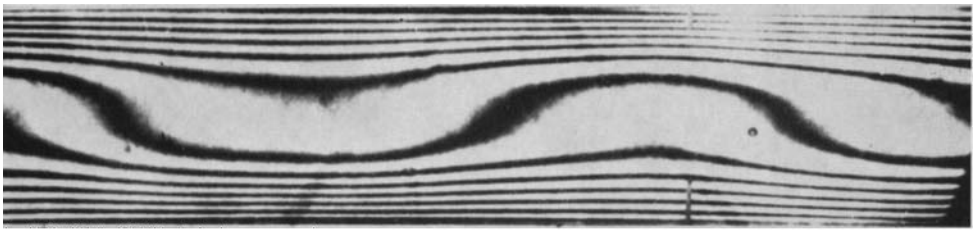

(*a*)

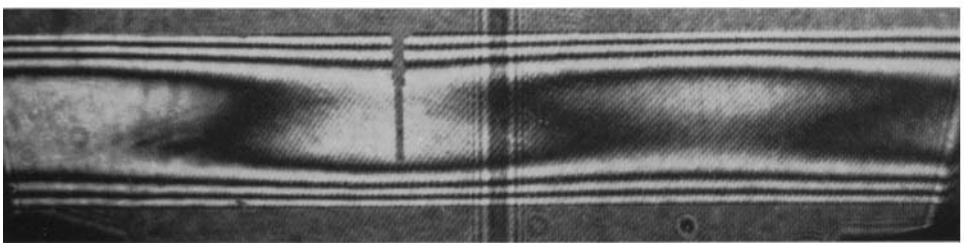

(*b*)

FIGURE 6. Laminar correction patterns. (*a*) Air; $Ra = 7{\cdot}0 \times 10^3$, $D = 1{\cdot}90$ cm, $\Delta T = 11{\cdot}10$ °C. (*b*) Water; $Ra = 9{\cdot}6 \times 10^3$, $D = 1{\cdot}27$ cm, $\Delta T = 0{\cdot}265$ °C.

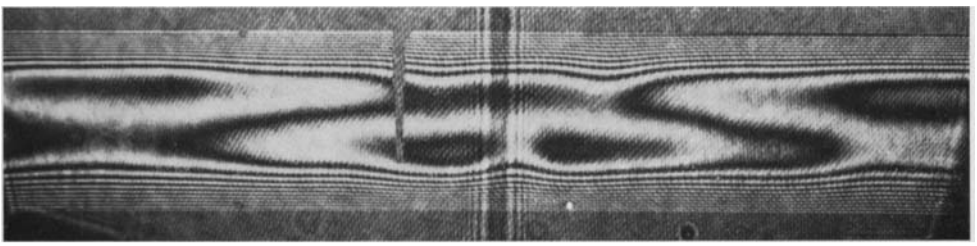

(*a*)

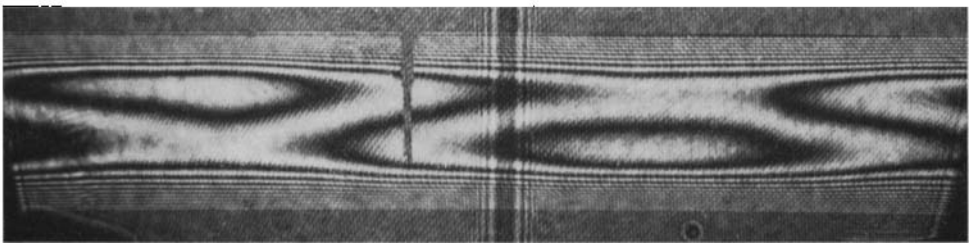

(*b*)

FIGURE 7. Laminar convection patterns in water. $Ra = 3{\cdot}15 \times 10^4$, $D = 1{\cdot}27$ cm, $\Delta T = 0{\cdot}857$ °C.

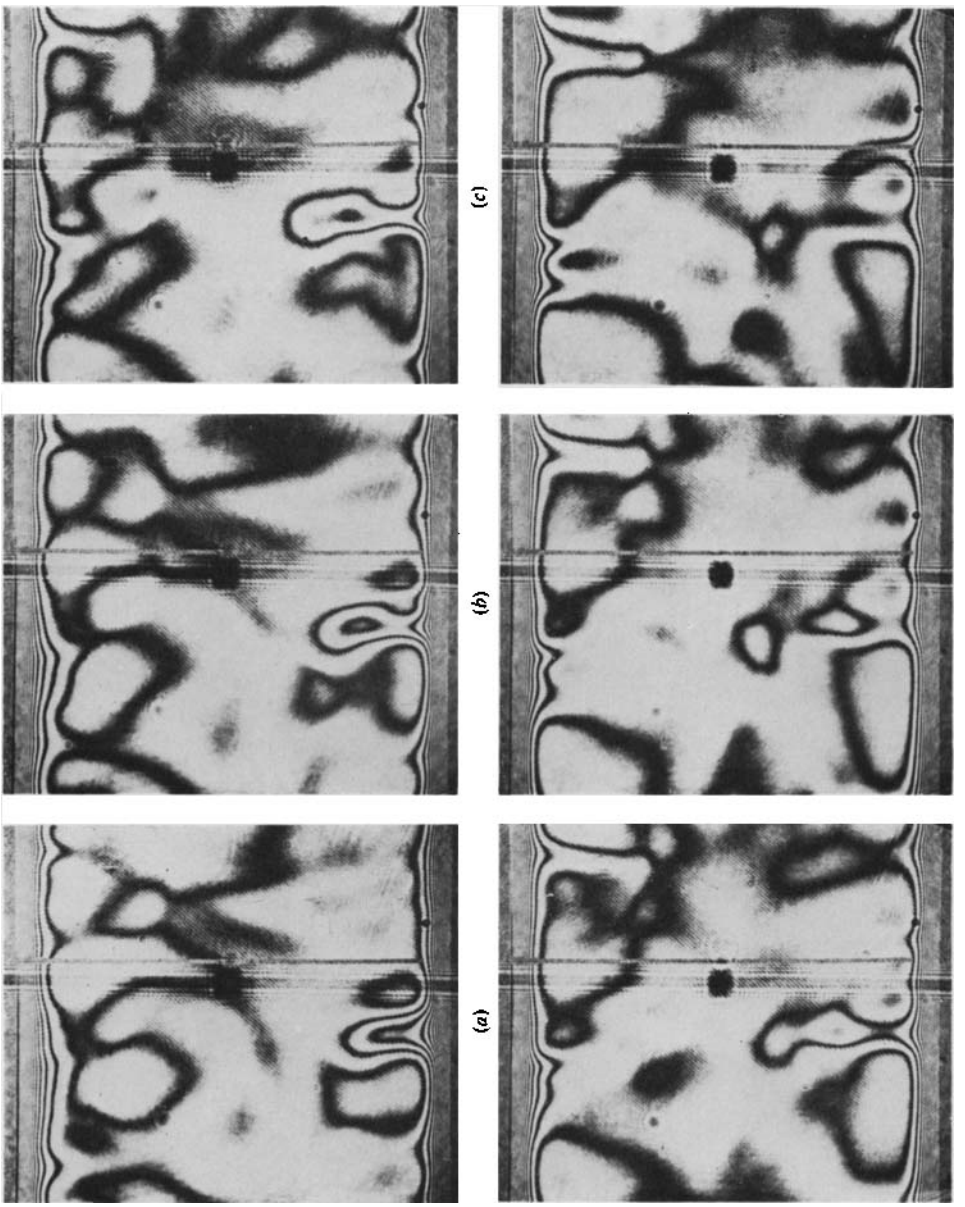

FIGURE 8. Release of a thermal from the boundary layer in water. 21 s sequence; $Ra = 2{\cdot}23 \times 10^6$, $D = 5{\cdot}07$ cm, $\Delta T = 1{\cdot}36$ °C.

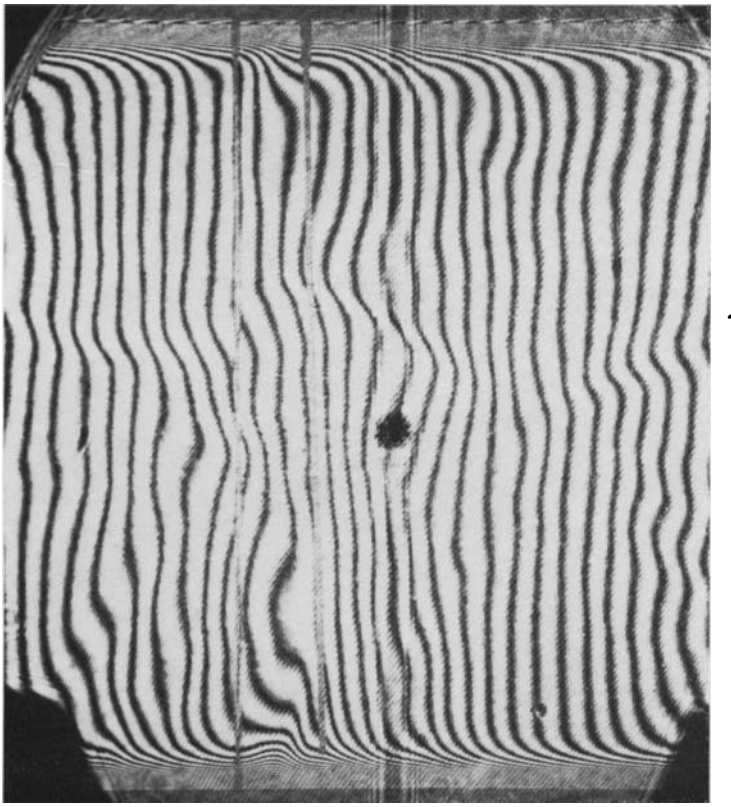

FIGURE 9. Moving front (ripples) in water layer. $Ra = 7{\cdot}10 \times 10^6$, $D = 6{\cdot}34$ cm, $\Delta T = 1{\cdot}39$ °C.

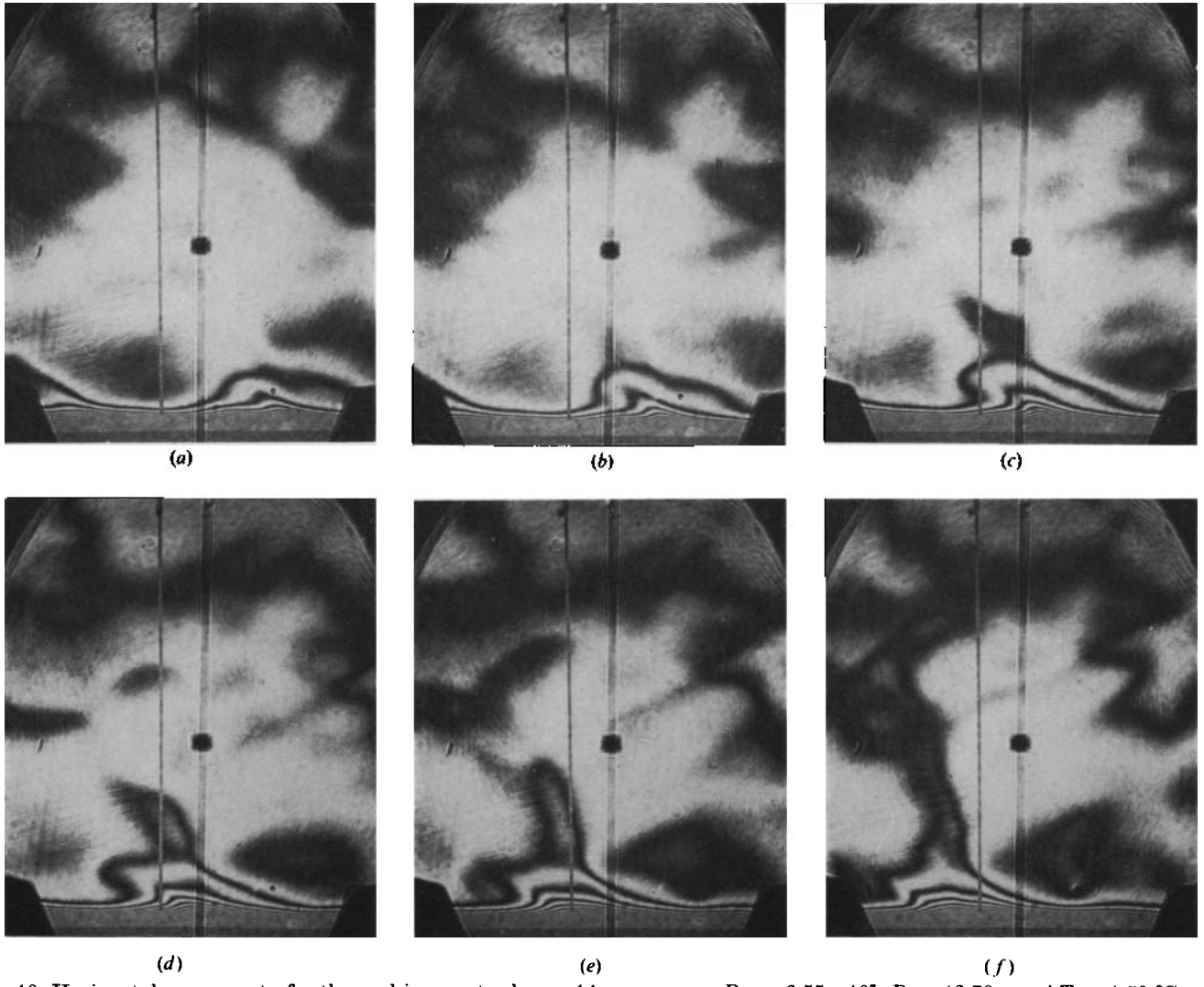

FIGURE 10. Horizontal movement of a thermal in a water layer. 14 s sequence; $Ra = 6{\cdot}55 \times 10^7$, $D = 12{\cdot}70$ cm, $\Delta T = 1{\cdot}59$ °C.

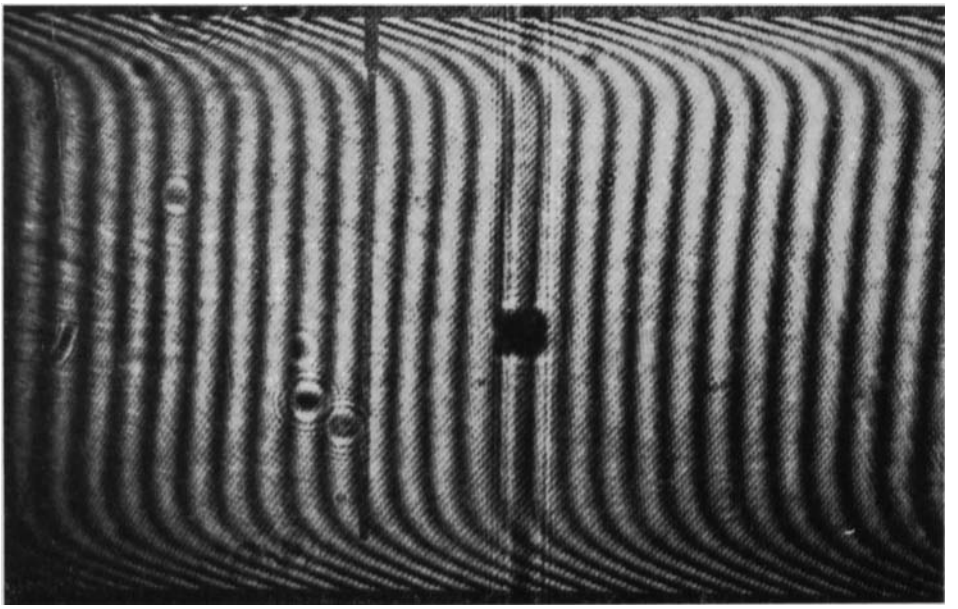

FIGURE 11. A time-averaged interferogram with a gradient reversal in a water layer. $Ra = 3{\cdot}11 \times 10^5$, $D = 3{\cdot}80$ cm, $\Delta T = 0{\cdot}311$ °C.